Draft version March 23, 2023
Typeset using LaTeX **preprint** style in AASTeX631

# Modelling Solar Oscillation Power Spectra: III. Spatiotemporal spectra of solar granulation velocity field as seen in SDO HMI Doppler-velocity measurements

Sergei V. Vorontsov,[1,2] Stuart M. Jefferies,[3] Jesper Schou,[4] and Timothy P. Larson[5]

[1] *Astronomy Unit, School of Physical and Chemical Sciences, Queen Mary University of London, Mile End Road, London E1 4NS, UK*

[2] *Institute of Physics of the Earth, B. Gruzinskaya 10, Moscow 123810, Russia*

[3] *Department of Physics and Astronomy, Georgia State University, Atlanta, GA, USA*

[4] *Max-Planck-Institut fur Sonnensystemforschung, Gottingen, Germany*

[5] *W.W. Hansen Experimental Physics Laboratory, Stanford University, Stanford, CA 94305-4085, USA*

## ABSTRACT

We suggest a physically motivated model of the uncorrelated background, which can be used to improve the accuracy of helioseismic frequency measurements. The basic assumption is that the correlation length of the convective motions is small compared with horizontal wavelength $R_\odot/\ell$ of the observations, where $\ell$ is degree of spherical harmonic $Y_{\ell m}(\theta,\varphi)$. When applied to solar power spectra at frequencies below acoustic resonances, the model reveals a distinct sensitivity to solar rotation: advection of the convective velocity pattern brings spatial correlations in the apparent stochastic velocity field (temporal correlations in the co-rotating frame induce spatial correlations in the inertial frame). The induced spatiotemporal correlations manifest themselves as antisymmetric component in the dependence of the convective noise power on azimuthal order $m$, which allows to address the solar differential rotation. With 360d power spectra measured with SDO HMI, three components of the rotation rate as a function of latitude can be addressed in a single measurement at $\ell = 300$. This result indicates that the model suggests a new way of measuring solar subsurface rotation, an approach which can complement traditional measurements based on correlation tracking.

*Keywords:* methods: data analysis — Sun: helioseismology — Sun: oscillations— Sun: rotation— Sun: convection

## 1. INTRODUCTION

The most difficult task in the contemporary helioseismology is to reduce systematic errors in solar p-mode frequencies. This problem stands up when analyzing results of prolonged measurements, which can only reduce random errors. A vast amount of data accumulated along the decades in dedicated ground-based and space projects call for a significant improvement of the data-analysis pipelene in order to employ their full diagnostic potential. For a recent overview of the available data and its processing, we refer the reader to Korzennik (2023).

Multiple sources of potential systematic errors come into play when we attempt to measure an oscillation frequency with accuracy better than the width of its resonant line in the observational

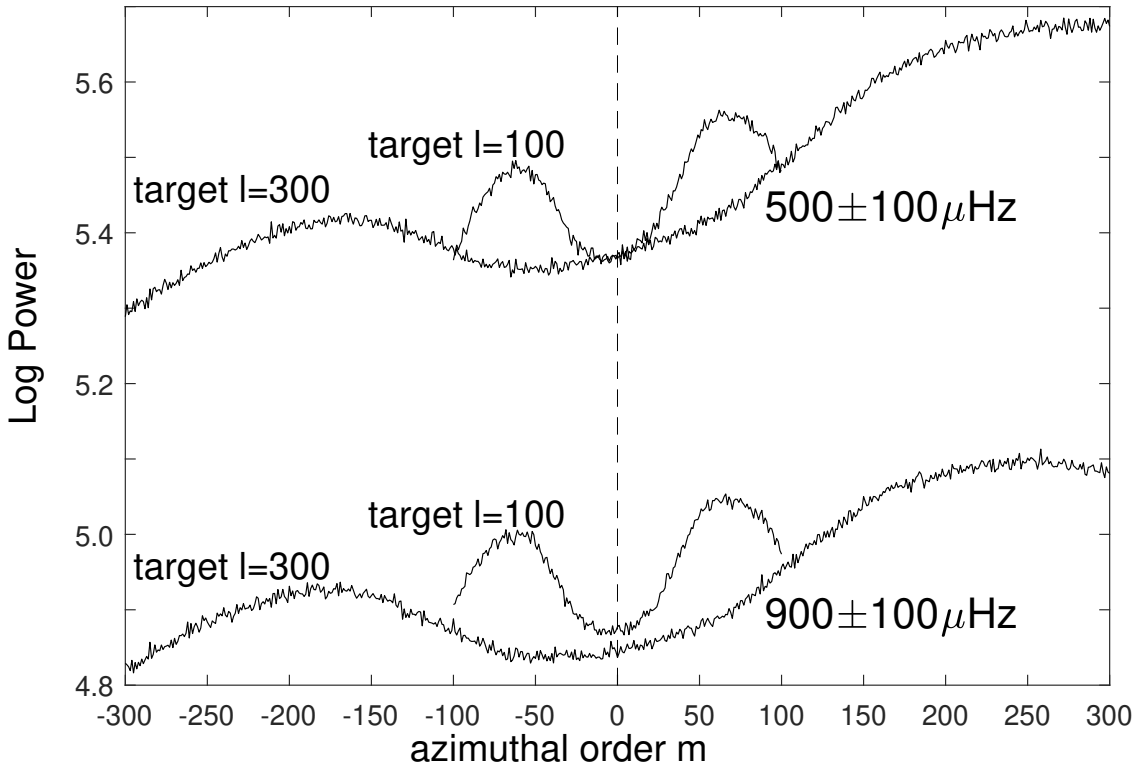


**Figure 1.** Observational noise power as function of azimuthal order $m$ at $l = 100$ and $l = 300$ measured at frequencies around $500\mu Hz$ (two upper curves) and $900\mu Hz$ (lower curves).

power spectrum. Systematic offset is caused by inadequate modeling of the asymmetric line profile, inaccurate treatment of nearby spatial leaks (inaccuracies in the leakage matrix, which in turn has to account for possible instrumental and optical distortions and mode-coupling effects), incorrect magnitude and/or frequency gradient of the uncorrelated background noise.

This study is focused on global modeling of the uncorrelated background. It is common practice in the peak-bagging procedures to account for the uncorrelated background by simply allowing it as a free parameter for each $(n, \ell)$ frequency multiplet (to ensure numerical stability, dependence on azimuthal order $m$ is usually ignored). We are looking for a possibility to describe the background in the entire range of $(n, \ell, m)$ globally by fitting a single function of frequency only, if observational data allows.

It is natural to start with addressing noise power in the frequency range uncontaminated by global oscillation resonances (below 1mHz, where solar f- and p-modes are buried below the noise level). In this study, we analyze power spectra obtained from 360d Doppler-velocity SDO HMI measurements (taken from 2019.03.14 onwards, the one-year period centered on solar activity minimum). Figure 1 shows the observed power at degree $\ell = 100$ and $\ell = 300$ as a function of $m$ at frequencies around $500\mu Hz$ and $900\mu Hz$; the measurements were averaged over $\pm 100\mu Hz$ frequency intervals.

We can make two interesting observations:

(i) two pairs of curves obtained at frequencies which differ by a factor two are essentially the same, the only difference is nearly-uniform vertical shift on the logarithmic scale. This feature indicates that

functional dependence of the noise power on spatial spectral numbers $(\ell, m)$ and temporal frequency $\omega$ is separable; and

(ii) the dependence on $m$ is highly asymmetric. This feature points immediately to effects of solar rotation, as sensitivity of the instrument does not depend on sign of $m$. With our sign convention, harmonics with $m$ positive are prograde waves, i.e. waves moving in the direction of rotation. In the co-rotating frame, these waves have smaller frequency; at smaller frequencies, the noise is higher.

Below is our attempt to understand this behavior in detail. In our vision, the noise comes from the turbulent convective velocity field in the solar photosphere. In Section 2, we address the spectral measures of this noise, assuming that the correlation length of the convective motions is small compared with observational wavelength $R_\odot/\ell$. We consider in detail the effects of differential rotation. In Section 3, we describe its measurement from the odd (in $m$) component of the noise power in SDO HMI measurements. We also analyze the even (in $m$) component, governed by different sensitivity of the instrument to different spatial harmonics of the velocity field. Extension of the leakage-matrix computations to include the response of the instrument to torsional components of the velocity field, which enter the analysis, is described in Appendix. Section 4 suggests an initial approximation for the noise power in the frequency domain of acoustic resonances, which has to be improved iteratively when fitting solar power spectra in frequency measurements. Our results are discussed in Section 5.

## 2. SPECTRAL MEASURES OF GRANULATION VELOCITY FIELD IN SPATIAL AND TEMPORAL DOMAINS

We work in a spherical coordinate system $(r, \theta, \varphi)$ aligned with solar rotation axis, and expand the time-dependent surface velocity field $\mathbf{v}(\theta, \varphi, t)$ in vector spherical harmonics

$$\mathbf{v}(\theta,\varphi,t) = \sum_{\ell,m} \left[ u_{\ell m}(t)\hat{r}Y_{\ell m}(\theta,\varphi) + v_{\ell m}(t)\nabla_1 Y_{\ell m}(\theta,\varphi) - w_{\ell m}(t)\hat{r}\times\nabla_1 Y_{\ell m}(\theta,\varphi)\right] \tag{1}$$

where $\nabla_1$ is angular part of gradient operator, $\nabla_1 = \hat{\theta}\partial/\partial\theta + \sin^{-1}\theta\hat{\varphi}\partial/\partial\varphi$, hats designate unit vectors, and make a Fourier transform of the time string of some large length $T$

$$\int_0^T e^{i\omega t}\mathbf{v}(\theta,\varphi,t)dt = \sum_{\ell,m} \left[ U_{\ell m}(\omega)\hat{r}Y_{\ell m}(\theta,\varphi) + V_{\ell m}(\omega)\nabla_1 Y_{\ell m}(\theta,\varphi) - W_{\ell m}(\omega)\hat{r}\times\nabla_1 Y_{\ell m}(\theta,\varphi)\right]. \tag{2}$$

Using orthogonality properties of vector spherical harmonics

$$\int\limits_{4\pi} [\nabla_1 Y^*_{\ell m}(\theta,\varphi)]\cdot[\nabla_1 Y_{\ell' m'}(\theta,\varphi)]\, d\Omega = \int\limits_{4\pi} [-\hat{r}\times\nabla_1 Y^*_{\ell m}(\theta,\varphi)]\cdot[-\hat{r}\times\nabla_1 Y_{\ell' m'}(\theta,\varphi)]\, d\Omega = \ell(\ell{+}1)\delta_{\ell'\ell}\delta_{m'm}, \tag{3}$$

where star designates complex conjugate, we have

$$U_{\ell m}(\omega) = \int_0^T e^{i\omega t}u_{\ell m}(t)dt = \int_0^T e^{i\omega t}dt \int_{4\pi} \mathbf{v}(\theta,\varphi,t)\cdot\hat{r}Y^*_{\ell m}(\theta,\varphi)d\Omega, \tag{4}$$

$$\ell(\ell+1)V_{\ell m}(\omega) = \int_0^T e^{i\omega t}v_{\ell m}(t)dt = \int_0^T e^{i\omega t}dt \int_{4\pi} \mathbf{v}(\theta,\varphi,t)\cdot\nabla_1 Y^*_{\ell m}(\theta,\varphi)d\Omega, \tag{5}$$

$$\ell(\ell+1)W_{\ell m}(\omega) = \int_0^T e^{i\omega t}w_{\ell m}(t)dt = \int_0^T e^{i\omega t}dt \int_{4\pi} \mathbf{v}(\theta,\varphi,t)\cdot[-\hat{r}\times\nabla_1 Y^*_{\ell m}(\theta,\varphi)]\, d\Omega \tag{6}$$

(these expressions are obtained by taking scalar product of both sides of Equation (1) with $\hat{r}Y^*_{\ell' m'}(\theta,\varphi)$, $\nabla_1 Y^*_{\ell' m'}(\theta,\varphi)$, and $-\hat{r}\times\nabla_1 Y^*_{\ell' m'}(\theta,\varphi)$, integrating in angular coordinates and taking the Fourier transform.)

We assume $\mathbf{v}(\theta,\varphi,t)$ to be a particular realization of a stationary stochastic process with zero mean. Quantities in the left-hand sides of Equations (4-6), represented by stochastic integrals in the right-hand sides, are thus random variables with zero mean, $E[U_{\ell m}(\omega)] = E[V_{\ell m}(\omega)] = E[W_{\ell m}(\omega)] = 0$. We are interested in evaluating their variances $VarU_{\ell m}(\omega) = E[U_{\ell m}(\omega)^* U_{\ell m}(\omega)]$, $VarV_{\ell m}(\omega)$ and $VarW_{\ell m}(\omega)$ (together with non-zero covariances, if any).

We associate $\mathbf{v}(\theta,\varphi,t)$ with turbulent velocity field of convective motions, imposed on a stationary large-scale background flow produced by differential rotation and meridional circulation. The basic assumption of our model is that for an observer moving together with the background flow, the convective velocities do not correlate in space. When addressing granulation velocity field, this assumption can only be relevant in a limited range of spherical harmonic degree $\ell$, when a typical size of a granule is small compared with horizontal wavelength $R_\odot/\ell$ (we will be working with Doppler-velocity power spectra in the degree range $0 \le \ell \le 300$). In this paper, we limit our analysis by the background flow produced by differential rotation only: effects of meridional circulation require different treatment and will be left for further studies.

To make derivations more transparent, we first consider a model with effects of rotation discarded, before generalizing the results to include effects of solid-body rotation and then differential rotation.

(i) *Non-rotating Sun.* Changing the order of integration, we rewrite Equation (4) as

$$U_{\ell m}(\omega) = \int_{4\pi} Y^*_{\ell m}(\theta,\varphi)\tilde{v}_r(\theta,\varphi,\omega)d\Omega, \tag{7}$$

where $\tilde{v}_r(\theta,\varphi,\omega)$ stands for the Fourier transform of radial velocity, $\tilde{v}_r(\theta,\varphi,\omega) = \int_0^T e^{i\omega t} v_r(\theta,\varphi,t)dt$, and consider the covariance

$$Cov\left[U_{\ell m}(\omega), U_{\ell' m'}(\omega)\right] = E\left[\int_{4\pi} Y_{\ell m}(\theta,\varphi)\tilde{v}^*_r(\theta,\varphi,\omega)d\Omega \times \int_{4\pi} Y^*_{\ell' m'}(\theta,\varphi)\tilde{v}_r(\theta,\varphi,\omega)d\Omega\right]. \tag{8}$$

Considering each of the two integrals in the right-hand side as a sum of integrals over small angular areas $\Delta\Omega_i$, and using indexing $\Delta\Omega_j$ to enumerate these areas in the same order in the second integral, we notice that the result is only contributed by diagonal elements $i = j$; expectation value of the cross-terms is zero because $\tilde{v}_r$-values do not correlate in space. We also know that the variance has a additive property. Therefore, if we replace the entire integration domain $4\pi$ in the right-hand side of Equation (8) by a small angular element $\Delta\Omega$, the result will be proportional to $\Delta\Omega$. We thus have

$$Cov\left[U_{\ell m}(\omega), U_{\ell' m'}(\omega)\right] = \int_{4\pi} Y_{\ell m}(\theta,\varphi)Y^*_{\ell' m'}(\theta,\varphi)\sigma_r^2(\omega)d\Omega = \delta_{\ell'\ell}\delta_{m' m}\sigma_r^2(\omega), \tag{9}$$

where

$$\sigma_r^2(\omega) = \lim_{\Delta\Omega\to 0}\frac{1}{\Delta\Omega}E\left[\int_{\Delta\Omega}\tilde{v}^*_r(\theta,\varphi)\tilde{v}_r(\theta,\varphi)d\Omega\right] \tag{10}$$

is positive spectral measure of the variance of vertical velocities, which we assume to be uniform over the solar surface.

We work in a similar manner with contribution of horizontal components of the velocity field $v_\theta(\theta,\varphi,t)$ and $v_\varphi(\theta,\varphi,t)$ which have corresponding Fourier transforms $\tilde{v}_\theta(\theta,\varphi,\omega)$ and $\tilde{v}_\varphi(\theta,\varphi,\omega)$.

We assume that horizontal velocities are isotropic in azimuthal direction and, therefore, the two orthogonal horizontal components do not correlate with each other and

$$\sigma_\theta^2(\omega) = \sigma_\varphi^2(\omega) = \frac{1}{2}\sigma_h^2(\omega), \tag{11}$$

where $\sigma_h^2(\omega)$ is spectral measure of absolute values of horizontal velocities. The result is

$$Cov\left[V_{\ell m}(\omega), V_{\ell' m'}(\omega)\right] = Cov\left[W_{\ell m}(\omega), W_{\ell' m'}(\omega)\right] == \frac{1}{2\ell(\ell+1)}\delta_{\ell'\ell}\delta_{m'm}\sigma_h^2(\omega) \tag{12}$$

(at $\ell = 0$, the horizontal components are identically zero). No cross-correlation is expected between $U$, $V$ and $W$-components, as they are produced by orthogonal components of the random velocity field.

We now extend the analysis to include the effects of rotation.

(ii) *Solid-body rotation.* In this scenario, the Sun rotates with uniform angular velocity $\Omega$ in the observational frame (the notation not to be confused with solid angle). We assume that in the co-rotating frame, the convective motions are not influenced by the rotation (i.e. the effects of Coriolis and centrifugal forces can be discarded, together with effects of rotational distortion of the background configuration). When the convective velocity field is observed in another reference frame, the only change is that due to advection: in the spherical-harmonic decomposition, a component of azimuthal order $m$ will have its temporal frequency shifted by $m\Omega$. The net result is that $\sigma_r^2(\omega)$ in Equation (9) has to be replaced with $\sigma_r^2(\omega - m\Omega)$, and similar with $\sigma_h^2(\omega)$ in Equation (12).

(iii) *Differential rotation.* We now allow the stationary rotation to change with latitude. When the rotation is uniform, the variance of $U_{\ell m}(\omega)$ can be written as

$$Var\, U_{\ell m}(\omega) = \frac{2\ell+1}{2}\frac{(\ell-m)!}{(\ell+m)!}\int_{-1}^{1}\left[P_\ell^m(z)\right]^2\sigma_r^2(\omega - m\Omega)\,dz, \quad z = \cos\theta. \tag{13}$$

Since contributions to the variance coming from different latitudes simply add up, the same expression will be valid when $\Omega$ in the right-hand side is allowed to depend on latitude. We will assume now that the rotation is slow; limiting the analysis by terms linear in $\Omega$,

$$\sigma_r^2\left(\omega - m\Omega(z)\right) = \sigma_r^2(\omega) - m\frac{d\sigma_r^2}{d\omega}\Omega(z), \tag{14}$$

and hence

$$Var\, U_{\ell m}(\omega) = \sigma_r^2\left(\omega - m\frac{2\ell+1}{2}\frac{(\ell-m)!}{(\ell+m)!}\int_{-1}^{1}\left[P_\ell^m(z)\right]^2\Omega(z)\,dz\right). \tag{15}$$

Following an approach which became standard in solar seismology since pioneering work of Ritzwoller & Lavely (1991), we represent $\Omega(z)$ by an expansion

$$\Omega(z) = \sum_{s=1,3,5,\ldots}\Omega_s\frac{dP_s(z)}{dz} \tag{16}$$

(note that only even components of $\Omega(z)$ enter our result, as $\left[P_\ell^m(z)\right]^2$ is even function of $z$).

The required angular integrals are

$$m\frac{2\ell+1}{2}\frac{(\ell-m)!}{(\ell+m)!}\int_{-1}^{1}\left[P_\ell^m(z)\right]^2\frac{dP_s(z)}{dz}\,dz=(-1)^{k+1}\frac{(\ell-1)!}{(\ell-k)!}\frac{(2\ell+1)!!}{(2\ell+2k-1)!!}\frac{(2k-1)!!}{(k-1)!}\mathcal{P}_{2k-1}^{(\ell)}(m)$$
$$=\left(\frac{4\pi}{2s+1}\right)^{1/2}\gamma_{s\ell}^m, \tag{17}$$

where $s=2k-1$, $\gamma_{s\ell}^m$ are odd polynomials of degree $s$ in $m$ defined in (Ritzwoller & Lavely 1991) and $\mathcal{P}_{2k-1}^{(\ell)}(m)$ are polynomials currently used in solar seismology to describe frequency splittimgs of solar oscillations, in normalization suggested in (Schou et al. 1994). Equation (17) can be derived by expanding $dP_s(z)/dz$ in $P_i(z)$, $i<s$, and evaluating integrals of triple products of Legendre polynomials. Convenient recurrence relations for evaluating $\mathcal{P}_{2k-1}^{(\ell)}(m)$ can be found in (Vorontsov 2007). We thus have

$$Var\,U_{\ell m}(\omega)=\sigma_r^2\left[\omega-\sum_{s=1,3,\ldots}\left(\frac{4\pi}{2s+1}\right)^{1/2}\gamma_{sl}^m\Omega_s\right]. \tag{18}$$

Introducing $a$-coefficients, commonly used in solar seismology, we have

$$Var\,U_{\ell m}(\omega)=\sigma_r^2\left(\omega-\sum_{s=1,3,\ldots}2\pi a_s\mathcal{P}_s^{(\ell)}(m)\right). \tag{19}$$

The relation between the expansion coefficients $\Omega_s$ and $a_s$ is provided by Aquation (17); in particular,

$$2\pi a_1=\Omega_1,\quad 2\pi a_3=-\frac{3(\ell-1)}{(2\ell+3)}\Omega_3,\quad 2\pi a_5=\frac{15(\ell-1)(\ell-2)}{2(2\ell+3)(2\ell+5)}\Omega_5. \tag{20}$$

Variances of $V_{\ell m}(\omega)$ and $W_{\ell m}(\omega)$ (Equations 5, 6) are transformed by the effects of differential rotation in exactly the same way.

We have an interesting observation: under effects of differential rotation, each spectral component of velocity variances "split" in its observed frequency in exactly the same way as an undistorted frequency of solar oscillations would split under effects of the same differential rotation, if influence of Coriolis forces can be discarded (leaving effects of advection only) and differential rotation does not change with depth.

We note also that possible inaccuracy, introduced by linearization in the rotation rate (Equations 14, 15) can only affect the response to differential component. The responce to the dominant $\Omega_1$-component is trated correctly whatever its magnitude, because $(4\pi/(2s+1))^{1/2}\gamma_{s\ell}^m=m$ for $s=1$.

## 3. SOLAR CONVECTIVE VELOCITY FIELD AS SEEN IN SDO HMI POWER SPECTRA

Instrumental response to different components of the velocity field does not depend on azimuthal order $m$. Parameters of differential rotation (Equations 19, 20) can thus be addressed by shifting in frequency the power spectra of individual $m$-channels in order to eliminate the odd (in $m$) component of the noise power. To account for a finite size of frequency window ($\pm 100\mu Hz$ in our measurement), this procedure was implemented in iterative way. The result obtained at $\ell=300$ at frequencies around

$900\mu Hz$ is $a_1 = \Omega_1/(2\pi) = 390.0 \pm 0.9$ nHz (synodic), $a_3 = 20.0 \pm 1.3$ nHz ($\Omega_3/(2\pi) = -13.4 \pm 0.9$ nHz), and $a_5 = 2.4 \pm 1.7$ nHz ($\Omega_5/(2\pi) = 1.3 \pm 0.9$ nHz). The merit function of this fit (defined as r.m.s. value of the residuals weighted with observational uncertainties, the uncertainties being evaluated under a standard assumption that observational power in individual channel at individual frequency has $\chi^2$-distribution with two degrees of freedom) is 1.073, which indicates that the targeted odd (in $m$) component is successfully eliminated in the "de-rotated" power spectra.

This result shall be compared with other available measurements. Helioseismic measurements of solar internal rotation loose their accuracy in the sub-surface layers, where the rotation varies rapidly with depth and global modes loose their resolving power. However, the measurements reduced to solar activity minimum (Figure 8 of Vorontsov et al. 2002) indicate the surface values of $\Omega_1/(2\pi) \simeq 435$ nHz (siderial, or synodic plus 31.6 nHz), $\Omega_3/(2\pi) \simeq -13$ nHz and $\Omega_5/(2\pi) \simeq 1$ nHz. The mean rotation rate $\Omega_1$ inferred from the convective noise is thus about 13 nHz slower; $\Omega_3$ and $\Omega_5$ appear to be in a perfect agreement.

A classical result of measuring solar differential rotation using correlation tracking (Snodgrass & Ulrich 1990) reads as $\Omega/(2\pi) = 0.473 - 0.077\cos^2\theta - 0.0575\cos^4\theta$ ($\mu$Hz) siderial, which translates to $\Omega_1/(2\pi) = 468.0$ nHz siderial, $\Omega_3/(2\pi) = -5.15$ nHz and $\Omega_5/(2\pi) = -1.46$ nHz. The variance with our measurement is much bigger here. One natural scenario is that the measurements refer to different effective depths below the visible solar surface. The result of Snodgrass & Ulrich (1990), however, is hard to reconcile with results of helioseismic measurements (e.g. Vorontsov et al. 2002), where $\Omega_3/(2\pi) \simeq -14 \pm 1$nHz is found to be nearly constant with depth over the entire convective envelope, and $\Omega_1/(2\pi)$ increases with depth, reaching its maximum value (at depth of about 6 percent of solar radius) of about 449 nHz (siderial) only.

With odd (in $m$) component successfully eliminated in the properly "de-rotated" observational power spectra, we now turn to the analysis of the remaining even component. For the same measurement at $\ell = 300$ and frequencies $900 \pm 100\mu$Hz, this component is shown by a thin line in Figure 2, where observational power

$$B^2_{\ell m}(\omega) = B^2_l(m)\overline{B}^2(\omega) \tag{21}$$

is represented in units of its $m$-averaged value $\overline{B}^2(\omega)$.

Contribution of the convective velocity field to the observational power spectra comes through multiple $U_{\ell m}$, $V_{\ell m}$ and $W_{\ell m}$-channels (Equations 4-6). As signals coming through these channels do not correlate with each other, we have, for the "de-rotated" power spectra,

$$B^2_{\ell m}(\omega) = \sigma^2_r(\omega) \sum_{\ell' m'} \left(R^{m'm}_{\ell'\ell}\right)^2 + \frac{\sigma^2_h(\omega)}{2\ell(\ell+1)} \left[\sum_{\ell' m'} \left(H^{m'm}_{\ell'\ell}\right)^2 + \sum_{\ell' m'} \left(T^{m'm}_{\ell'\ell}\right)^2\right], \tag{22}$$

where we introduce the notation $R$, $H$ and $T$ to designate separate leakage matrices which specify sensitivity coefficients of the instrument to radial components of the velocity field, horizontal components of the poloidal vector fields, and components of the toroidal fields (Equation 1), respectively. To make sure that sufficient amount of spectral leaks are accounted for, the leakage matrices were computed with $\ell'$ in the range $\ell \pm 30$ and $m' = m \pm 30$. Computation of the leakage matrices followed a semi-analytic approach described in (Vorontsov & Jefferies 2005), which was generalized to include the response of the instrument to toroidal velocity fields; the details can be found in Appendix. To account for a finite resolution of the instrument in the CCD plane, the leakage-matrix analysis

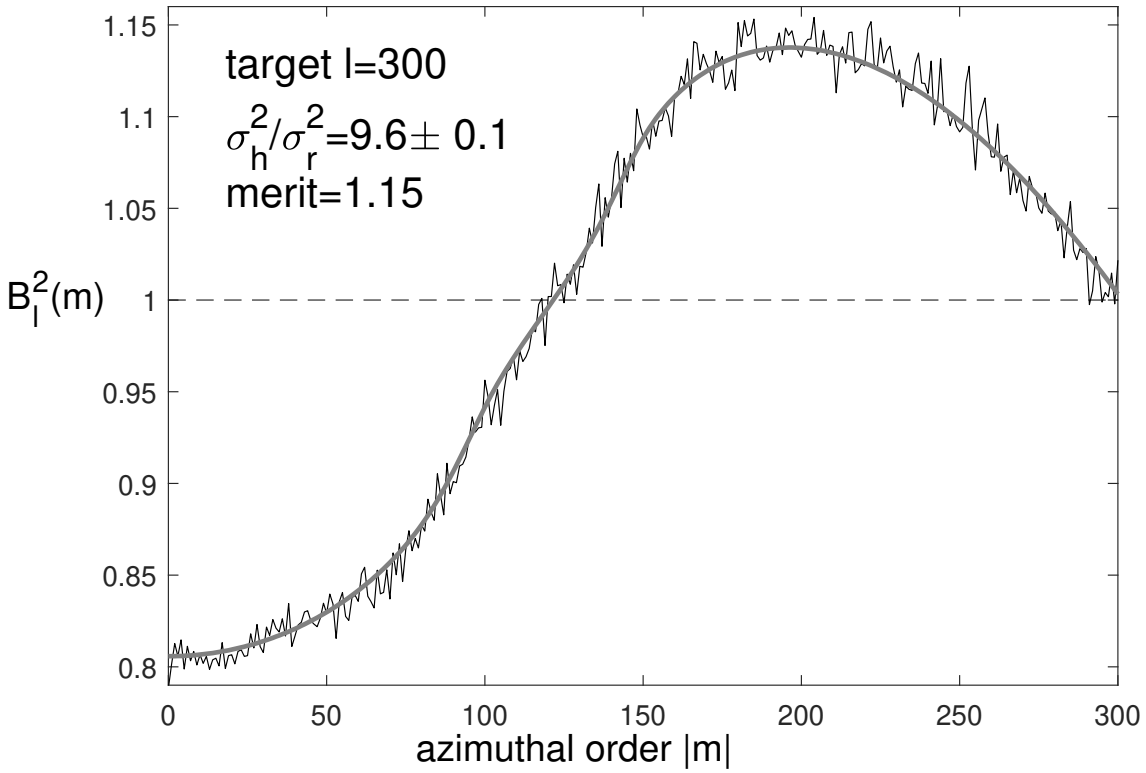


**Figure 2.** Even component in the observational noise power as function of azimuthal order $m$ at $l = 300$ measured at frequencies around $900\mu Hz$ (thin line). Thick gray line shows its approximation obtained by fitting synthetic power.

involves convolution of the images with a 2D Gaussian point-spread function (PSF); when working with high-resolution HMI data in the intermediate-degree range $\ell \leq 300$, the width of the PSF was set to zero (infinite resolution, PSF described by 2D Dirac $\delta$-function). Solar B-angle was set to 5.11 deg, the r.m.s. value of its annual variation (for a small B-angle, its effect is quadratic in its magnitude).

Observational power $B^2_{\ell m}(\omega)$ considered as a function of $m$ at $\ell = 300$ is fitted by a linear combination of the two terms in the right-hand side of Equation (22) with unknown coefficients $\sigma_r^2$ and $\sigma_h^2$. The result is shown in Figure 2 by a thick gray line. Visual inspection of the fit quality and the value of the corresponding merit function both indicate that the approximation of the measured function of $m$ by a linear combination of two functions coming exclusively from leakage-matrix analysis is perfectly adequate. The inferred ratio $\sigma_h^2/\sigma_r^2 = 9.6 \pm 0.1$ indicates that horizontal velocities in the turbulent flow are about 3 times bigger than vertical velocities. The fit quality remains to be adequate when the same analysis is applied to data at smaller degree $\ell$. An interesting observation is that the measured ratio $\sigma_h^2/\sigma_r^2$ increases monotonically to $18.2 \pm 0.5$ at $\ell = 100$ and $20.5 \pm 2.9$ at $\ell = 5$ (at degree $\ell < 5$, this measurement looses stability due to insufficient number of the available $m$-states). This finding may indicate that bigger convective cells have bigger average ratio of horizontal to vertical velocities.

Another finding is that the observed $m$-averaged value $\overline{B}^2(\omega)$ stays nearly constant in the entire degree range: it drops monotonically when going from $\ell = 0$ to $\ell = 300$, but only by about 15 percent

(for a comparison, in medium-$\ell$ SOHO MDI measurements of much smaller spatial resolution, this variation amounts to two orders of magnitude). This behavior indicates that in the degree range of up to $\ell = 300$ the spatial resolution of the HMI instrument is indeed almost perfect. To clarify this point, our analysis can be made independent on the leakage-matrix computations—assuming, of coarse, that the spatial resolution of the instrument is perfect.

In addition to the coordinate system $(\theta, \varphi)$ with $z$-axis aligned with solar rotation axis, we introduce another coordinate system $(\theta', \varphi')$ with $z'$-axis (from which $\theta'$ is counted) directed from the Sun towards the observer. Considering the projection of the turbulent velocity field $\mathbf{v}(\theta, \varphi, t)$ (Equation (1) on the CCD plane directly, without its decomposition in vector spherical harmonics, we have

$$B^2_{\ell m}(\omega) = E \left| \int_{4\pi} Y^*_{\ell m}(\theta, \varphi) \Pi(sin\theta') \hat{z}' \cdot \tilde{\mathbf{v}}(\theta, \varphi, \omega)\, d\Omega \right|^2, \tag{23}$$

where $\tilde{\mathbf{v}}(\theta, \varphi, \omega)$ is Fourier transform of $\mathbf{v}(\theta, \varphi, t)$ at frequency shifted by advection effects, and $\Pi(sin\theta')$ is apodization function, $\sin\theta'$ being radial coordinate in the image plane in units of apparent solar radius. Evaluating the measure of the stochastic signal in a way described in Section 2 gives immediately

$$B^2_{\ell m}(\omega) = \int_{4\pi} Y^*_{\ell m}(\theta, \varphi) Y_{\ell m}(\theta, \varphi) \Pi^2(\sin\theta') \left[ \cos^2\theta' \sigma^2_r(\omega) + \frac{1}{2} \sin^2\theta' \sigma^2_h(\omega) \right] d\Omega, \tag{24}$$

where $\cos^2\theta'$ and $\sin^2\theta'/2$ account for the line-of-sight projection effects. Using addition theorem for spherical harmonics, the $m$-averaged value is

$$\overline{B}^2(\omega) = \frac{1}{2\ell + 1} \sum_{m=-\ell}^{\ell} B^2_{\ell m}(\omega) = \frac{1}{4\pi} \int_{4\pi} \Pi^2(\sin\theta') \left[ \cos^2\theta' \sigma^2_r(\omega) + \frac{1}{2} \sin^2\theta' \sigma^2_h(\omega) \right] d\Omega, \tag{25}$$

the result which does not depend on the target degree $\ell$.

By expanding $\cos^2\theta' \Pi^2(\sin\theta')$ and $\sin^2\theta' \Pi^2(\sin\theta')$ in Equation(24) in spherical harmonics and transforming the result to $(\theta, \varphi)$-coordinates, it is also possible to evaluate the right-hand side at individual $m$-values. We skip the details of this analysis, as its principal motivation was to cheque the accuracy of our leakage-matrix computations. The numerical results of the two approaches went out to be the same.

The slight variation of the apparent values of $\overline{B}^2(\omega)$ with degree $\ell$ indicates that the leakage matrices can be somewhat improved by setting the PSF width to a small but non-zero value. We conclude that the measurements of the solar noise can be used to calibrate the effective PSF of the instrument. This option may be particularly interesting for analyzing data obtained with SOHO MDI instrument.

## 4. TEMPORAL DOMAIN

The $m$-average of the of the de-rotated (frequency-shifted according to the result of differential-rotation measurement) power spectra in the entire frequency domain of SDO HMI data at $\ell = 300$ is shown in Figure 3.

At frequencies less than about $100\mu$Hz, variation of the observed power with $\ell$ and $m$ can not be explained by our model, which looses its ability to fit the data with any reasonable accuracy. It looks as if our basic assumption of negligibly small correlation length gets violated by convective motions of supergranular scale. We leave this extremely interesting spatiotemporal domain to further studies.

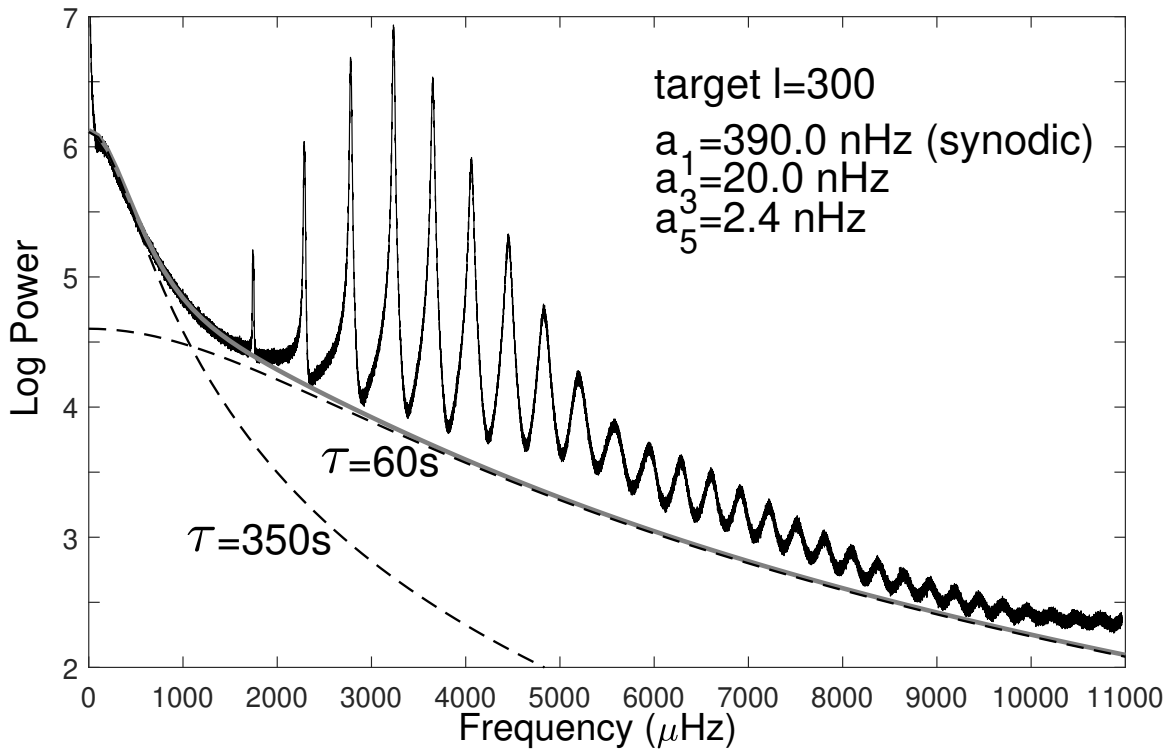


**Figure 3.** De-rotated and $m$-averaged SDO HMI power spectrum at $l = 300$ (thin line). Dashed lines show two simple models (see text); their sum is shown by thick gray line.

In this study, the data analysis was limited by frequencies below the oscillation resonances. We can hope that the dependence of the noise power on $\ell$ and $m$ (the $B^2_\ell(m)$) measured in this frequency range will stay the same at higher frequencies; this assumption, of coarse, remains to be verified by addressing residuals of spectral fitting procedures. We note that at frequencies from about 3 mHz and higher, the measurement of the background component is difficult because the signal-to-noise ratio of acoustic resonances becomes very high. At these frequencies, it is now the uncorrelated background which gets buried below the resonant power.

We can suggest a simplistic model for the frequency dependence of the background noise $\overline{B}^2(\omega)$ to be used as initial guess in the peak-bagging procedures. Imagine a convective eddy emerging on the solar surface from below at time $t = 0$. Let the observed velocity increases linearly with time and then drops exponentially,

$$v = \begin{cases} 0, & t < 0 \\ \frac{t}{\tau^2} e^{-\frac{t}{\tau}}, & t \geq 0. \end{cases} \tag{26}$$

Taking the Fourier transform, the observed power is $(1 + \omega^2\tau^2)^{-2}$. The Fourier power is a cosine Fourier transform of the autocorrelation function, which is

$$ACF = \frac{1}{4\tau} \left(1 + \left|\frac{t}{\tau}\right|\right) e^{-|\frac{t}{\tau}|}. \tag{27}$$

We adjust a linear combination of these "seismic events" with two different values of $\tau$ to approximate the expected variation of the uncorrelated background in the entire frequency range; the result is

shown in Figure 3 by two dashed lines for the two separate components and by thick gray line for their sum. The fitted values of $\tau$, about 1 min and 6 mins, do not contradict the lifetimes of solar granules. A relative excess of observational power at highest frequencies may be due to aliasing signal coming from frequencies higher than Nyquist frequency.

## 5. DISCUSSION

Implementation of our model in frequency measurements is rather straightforward. At each degree $\ell$, the even functions $B^2_\ell(m)$ are measured from the de-rotated power spectra, around some frequency which is below all the detectable resonances. The initial approximation for the frequency dependence of the uncorrelated background $\overline{B}^2(\omega)$ is then improved by fitting individual multiplets in the power spectra. When the resolution of the instrument is not perfect (HMI measurements at higher degree $\ell$ or SOHO MDI measurements), the smaller sensitivity to modes of higher degree $\ell$ will be captured in $B^2_\ell(m)$.

The suggested measurement of differential rotation from power spectra at frequencies below the acoustic resonances will benefit from employing more data of smaller and higher degree $\ell$ analyzed in different frequency intervals. It is interesting to extend these measurements to datasets obtained at different time to address temporal variations of the subsurface differential rotation ("torsional oscillations").

In our limited exercise with observational data, we already have two other interesting findings, which deserve more extensive data analysis. The inferred mean rotation rate increases monotonically when target degree $\ell$ gets smaller: it may indicate that we are capturing signal from bigger convective sells, which are rooted deeper below the photosphere, where the background rotation is faster. The inferred ratio $\sigma^2_h/\sigma^2_r$ has a clear tendency to get bigger when $\ell$ gets smaller; it indicates that in bigger convective sells, horizontal velocities become more dominant.

Our model becomes inconsistent with observations quite rapidly at frequencies from about $100\mu$Hz and below. In our understanding, our basic assumption of small correlation length breaks down when observations start to feel signals from supergranular convective sells. More sophisticated approach is needed to deal with turbulent-velocity correlations simultaneously in both space and time.

## APPENDIX

The leakage matrices used in this study were calculated using semi-analytic approach described in (Vorontsov & Jefferies 2005). This approach was extended in (Vorontsov & Jefferies 2013) to account explicitly for non-zero solar B-angle. In this study, we need to extend the analysis further to address the response of the instrument to components of the velocity field described by toroidal vector spherical harmonics. We have also noticed an inaccuracy in the earlier treatment of the B-angle effect (line-of-sight projection was done in the direction orthogonal to solar rotation axis, thus missing the observer). Therefore, we outline briefly the overall algorithm, adding proper extensions.

We implement three separate leakage matrices—$R^{m'm}_{\ell'\ell}$, $H^{m'm}_{\ell'\ell}$ and $T^{m'm}_{\ell'\ell}$, with response coefficients to the vertical component of poloidal vector fields, to their horizontal component, and to the toroidal vector fields, respectively. We discard here all possible instrumental and optical distortions.

We choose the coordinate system $(r, \theta, \varphi)$ such that its $z$-axis is aligned with solar rotation, axis $y$ is orthogonal to the line of sight, and axis $x$ (from which $\varphi$ is counted) is directed towards the observer

when solar B-angle is zero. We choose another axis $z'$ which points towards the observer. Angle $\beta$ counted from $z$ to $z'$ is 90 degrees minus solar B-angle. We start with line-of-sight projection of the vector velocity fields: it will allow further analysis to work with scalar fields. Projection of vector $\mathbf{v}$ to the line of sight is

$$\hat{z}' \cdot \mathbf{v} = \sin\beta\, \hat{x} \cdot \mathbf{v} + \cos\beta\, \hat{z} \cdot \mathbf{v}. \tag{1}$$

For poloidal vector fields, we need an expansion in spherical harmonics of $\hat{x} \cdot \hat{r} Y_{\ell m}(\theta, \varphi)$, $\hat{z} \cdot \hat{r} Y_{\ell m}(\theta, \varphi)$, $\hat{x} \cdot \nabla_1 Y_{\ell m}(\theta, \varphi)$, and $\hat{z} \cdot \nabla_1 Y_{\ell m}(\theta, \varphi)$. These decompositions are listed by Equations (45, 47, 42, 44) of (Vorontsov & Jefferies 2005). Corresponding expressions for toroidal vector spherical harmonics are derived in the same way; the result is

$$\hat{x} \cdot [-\hat{r} \times \nabla_1 Y_{\ell m}(\theta, \varphi)] = -\frac{i}{2} \left[(\ell + m)(\ell - m + 1)\right]^{\frac{1}{2}} Y_{\ell, m-1}(\theta, \varphi) - \frac{i}{2} \left[(\ell - m)(\ell + m + 1)\right]^{\frac{1}{2}} Y_{\ell, m+1}(\theta, \varphi), \tag{2}$$

$$\hat{z} \cdot [-\hat{r} \times \nabla_1 Y_{\ell m}(\theta, \varphi)] = -imY_{\ell, m}(\theta, \varphi). \tag{3}$$

The rest of the analysis is the same as in (Vorontsov & Jefferies 2005, 2013): we rotate the coordinate system by angle $\beta$ to direct axis $z$ towards the observer, convolve the image with PSF in the apodization domain, and rotate the coordinate system back to its original orientation. Symmetry relations for the resulted leakage matrices are

$$R_{\ell'\ell}^{-m',-m} = (-1)^{m'+m} R_{\ell'\ell}^{m'm}, \quad H_{\ell'\ell}^{-m',-m} = (-1)^{m'+m} H_{\ell'\ell}^{m'm}, \quad T_{\ell'\ell}^{-m',-m} = (-1)^{m'+m+1} T_{\ell'\ell}^{m'm}. \tag{4}$$

## REFERENCES


Korzennik, S. G., 2023, Frontiers in Astron. & Space Sci., 9, id.1031313

Ritzwoller, M. H., & Lavely, E. M. 1991, ApJ, 369, 557

Schou, J., Christensen-Dalsgaard, J., Thompson, M. J., 1994, ApJ, 433, 389

Snodgrass, H. B., & Ulrich, R. K., 1990, ApJ, 351, 309

Vorontsov, S. V., Christensen-Dalsgaard, J., Schou, J., Strakhov, V. N., Thompson, M. J., 2002, in: From Solar Min to Max: Half a Solar Cycle with SOHO, ed. A. Wilson, Proc. *SOHO* 11 Symposium (ESA SP-508; Noordwijk: ESA), 111

Vorontsov, S. V., & Jefferies, S. M., 2005, ApJ, 623, 1202

Vorontsov, S. V., & Jefferies, S. M., 2013, ApJ, 778, 75

Vorontsov, S. V. 2007, MNRAS, 378, 1499